Day and Night-Time Dehazing by Local Airlight Estimation

Cosmin Ancuti, *Member, IEEE*, Codruta O. Ancuti, *Member, IEEE*, Christophe De Vleeschouwer, *Member, IEEE*, and Alan C. Bovik

***Abstract*— We introduce an effective fusion-based technique to enhance both day-time and night-time hazy scenes. When inverting the Koschmieder light transmission model, and by contrast with the common implementation of the popular dark-channel [1], we estimate the airlight on image patches and not on the entire image. Local airlight estimation is adopted because, under night-time conditions, the lighting generally arises from multiple localized artificial sources, and is thus intrinsically non-uniform. Selecting the sizes of the patches is, however, non-trivial. Small patches are desirable to achieve fine spatial adaptation to the atmospheric light, but large patches help improve the airlight estimation accuracy by increasing the possibility of capturing pixels with airlight appearance (due to severe haze). For this reason, multiple patch sizes are considered to generate several images, that are then merged together. The discrete Laplacian of the original image is provided as an additional input to the fusion process to reduce the glowing effect and to emphasize the finest image details. Similarly, for day-time scenes we apply the same principle but use a larger patch size. For each input, a set of weight maps are derived so as to assign higher weights to regions of high contrast, high saliency and small saturation. Finally the derived inputs and the normalized weight maps are blended in a multi-scale fashion using a Laplacian pyramid decomposition. Extensive experimental results demonstrate the effectiveness of our approach as compared with recent techniques, both in terms of computational efficiency and the quality of the outputs.**

***Index Terms*— Local airlight, haze, dehazing, night-time, fusion.**

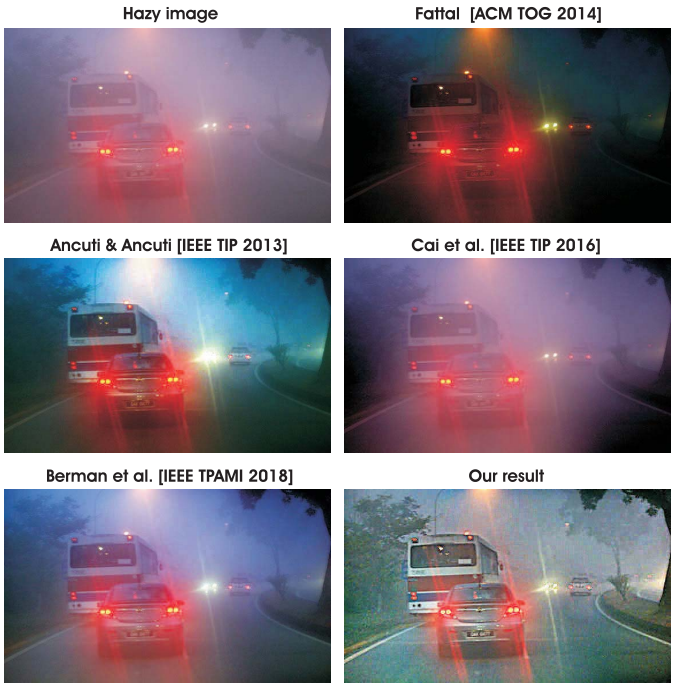

Fig. 1. Night-time scene capture is a challenging task under difficult weather conditions and recent single-image dehazing techniques [2]–[5] suffer from important limitations when applied to such images.

I. Introduction

OUTDOOR images often suffer from poor visibility introduced by weather conditions, such as haze or fog. Haze is a common atmospheric phenomena produced by small floating particles that absorb and scatter the light from its propagation direction. Due to attenuation and scattering, hazy scenes are characterized by poor contrast of distant objects, color shifting, and additional noise. Outdoor applications such as video surveillance and automatic driving assistance require good restoration of such distorted images.

The process of removing haze effects from images (dehazing) is an ill-posed problem. First attempts tackled it by using additional information such as rough depth [6] of the scene or multiple images [7]. More recently, several techniques [1]–[3], [8]–[16], have introduced solutions that do not require any additional information than the single input hazy image. While the effectiveness of these techniques has been extensively demonstrated on daylight hazy scenes, they suffer from important limitations on night-time hazy scenes.

Obviously, the problem of dehazing of night-time scenes is more challenging. This is mainly due to the multiple light sources that cause a strongly non-uniform illumination of the scene. As a result, the night-time dehazing problem has been addressed only by a limited number of researchers [17]–[19], who introduced methods specific to night-time conditions. As may be seen in Fig. 1 and also in the experimental section, state-of-the-art dehazing techniques designed in general for

Manuscript received August 8, 2019; revised January 3, 2020, February 10, 2020, and March 26, 2020; accepted March 26, 2020. Date of publication April 23, 2020; date of current version May 8, 2020. This work was supported in part by the 2020 European Union Research and Innovation Horizon 2020 through the grant agreement Marie Sklodowska-Curie (TECNIOspring PLUS) under Grant 712949 and in part by the Agency for the Competitiveness of the Company of the Generalitat de Catalunya under Grant ACCIO: TECSPR17-1-0054. The associate editor coordinating the review of this manuscript and approving it for publication was Prof. Dong Xu. *(Cosmin Ancuti and Codruta O. Ancuti contributed equally to this work.) (Corresponding author: Codruta O. Ancuti.)*

Cosmin Ancuti is with the ETcTI, Universitatea Politehnica Timisoara, 300006 Timişoara, Romania, and also with the Institute of Informatics and Applications, University of Girona, 17004 Girona, Spain (e-mail: cosmin.ancuti@upt.ro).

Codruta O. Ancuti is with the ETcTI, Universitatea Politehnica Timisoara, 300006 Timişoara, Romania (e-mail: codruta.ancuti@gmail.com).

Christophe De Vleeschouwer is with the ICTEAM, Universite Catholique de Louvain, 1348 Ottignies-Louvain-la-Neuve, Belgium.

Alan C. Bovik is with the Department of Electrical and Computer Engineering, The University of Texas at Austin, Austin, TX 78712 USA.

Digital Object Identifier 10.1109/TIP.2020.2988203

day-time dehazing perform poorly for the task of night-time dehazing.

In this paper, we introduce an effective fusion-based technique to enhance the visibility of hazy scenes both in day or night conditions. The technique presented here builds on our preliminary version, which was specific to night dehazing [20]. In this extended version we generalize our solution to work effectively both on day and night-time hazy scenes. To the best of our knowledge, this is the first algorithm that demonstrates competitive results simultaneously on the most representative day-time and night-time dehazing datasets.

Therefore, we introduce a novel and general way to compute the airlight component required to invert the Koschmieder's light transmission model [21]. Specifically, to account for non-uniform illumination, we propose to compute this value locally, on patches of varying sizes. This is especially relevant in night-time conditions, when the lighting results from multiple artificial sources, and is thus intrinsically non-uniform. In practice, the same approach as the one recommended by the dark channel prior is adopted to estimate the airlight on each patch, based on the color of most hazy pixels, identified as brightest ones [1]. A critical issue, however, lies in the patch size selection. Small patches are desirable to achieve fine spatial adaptation, but small patches might also lead to inaccurate airlight estimates due to the unavailability of pixels affected by strong haze when the patch becomes too small. For this reason, we deploy multiple patch sizes, each generating a single input to a subsequent multi-scale fusion process.

Our fusion approach is accomplished in three main steps. First, based on our local airlight estimation method using different patch sizes, we derive the first two inputs of the fusion approach. To reduce the glowing effect and emphasize the finest details of the scene, the third input is defined to be the Laplacian of the original image. In the second step, the important features of these derived inputs are filtered based on several quality weight maps (local contrast, saturation and saliency). Finally the derived inputs and the normalized weight maps are blended in a multi-scale fashion, using a Laplacian pyramid decomposition of the inputs and a Gaussian pyramid of the normalized weights. In addition to being effective in night-time conditions, our approach appears to naturally generalize to day-time scenes, by increasing the size of the patches in response to increased contrast and a wider distribution of color in the original image.

The experimental section validates our technique on a diverse set of day-time and night-time hazy scenes. It demonstrates the value of our approach as compared to recent techniques, both in terms of computational efficiency, and enhanced image quality.

II. Background Theory and Related Work

A. Observation Model

As in previous dehazing methods [1], [8], [16], [22]–[24] light propagation is expressed by Koschmieder's model [21], which has been shown to provide a reasonable approximation of atmospheric effects on light reaching the camera.

In short, it states that the light intensity $\mathcal{I}$ at each image coordinate x is the result of two main additive components - *direct transmission* $\mathcal{D}(x)$ and *airlight* $\mathcal{A}(x)$:

$$\mathcal{I}(x) = \mathcal{D}(x) + \mathcal{A}(x) = \mathcal{J}(x)\ T\ (x) + A_\infty\ [1 - T\ (x)] \quad (1)$$

where $\mathcal{J}(x)$ is the scene radiance or haze-free pixel color, $T(x)$ is the transmitivity along the cone of vision, and A_∞ is the atmospheric intensity, resulting from the environmental illumination.

The *airlight* $\mathcal{A}(x)$ is the main cause of color shifting and is expressed as:

$$\mathcal{A}(x) = A_\infty\ [1 - T\ (x)] \quad (2)$$

The transmission $T(x)$ represents the amount of light that has been transmitted between observed surface and the camera. Assuming a homogeneous medium, $T(x)$ is approximated:

$$T\ (x) = e^{-\beta\ d(x)} \quad (3)$$

where β is the medium attenuation coefficient due to scattering, and $d(x)$ represents the distance between the camera and the physical point associated with pixel coordinate x. Practically, the dehazing problem consists in estimating the latent image $\mathcal{J}$ only from the hazy input image $\mathcal{I}$. It is a mathematically ill-posed problem, since, in addition to $\mathcal{J}$, the transmission T and the atmospheric intensity A_∞ are also unknown.

B. Related Work

As previously discussed, most dehazing methods have focused on day-time scenes. Early dehazing techniques employ additional information. For instance [25], [26], [7] consider an atmospheric scattering model to derive geometric constraints on scene color changes caused by varying atmospheric conditions. They then exploit those constraints to recover the *true* scene colors from multiple images taken under different, but unknown, weather conditions.

Other strategies use information about the 3D scene geometry. Narasimhan and Nayer [7] employ an approximated depth-map specified interactively by the users while the more recent *Deep Photo* [6] system uses existing georeferenced digital terrain and urban models to restore such spoiled images. Polarization methods [27], [28], take advantage of the fact that the path radiance (airlight) is partially polarized. They typically process multiple images of the same scene acquired with different states of a mounted polarizer [29], [30]. The difference between different polarized inputs enables the estimation of the haze light component. In general, all these dehazing strategies that employ additional information are usually impractical to deploy.

Therefore, a number of studies have attempted to restore hazy scenes using only the information from a single hazy input image. Various single image-based strategies [1], [8]–[10], [16], [22]–[24], [31], [32] have been introduced in the recent years. A first category among these is represented by those methods that restore visibility without employing any physical model. Tan [9] introduces a method that maximizes the local contrast while constraining the image intensity to be

smaller than the global atmospheric light value. The contrast-based enhancing approach of Tarel and Hautière [10] is a computationally effective technique, but requires the depth-map to be smooth except along edges. In [13], hazy regions are filtered by a simple per-pixel operation to estimate the airlight and the transmission map. Ancuti and Ancuti [3] introduced a simple but effective multi-scale fusion strategy that combines multiple images derived from the original input, with the aim of recovering the visibility of each region of the scene in at least one of the multiple images. This strategy has been recently extended by Choi *et al.* [33]. Those methods make use of measurable deviations from statistical regularities observed in natural foggy and fog-free images, to predict a local fog density index for the entire image. This fog density index is then used to improve the contrast in the images. More recently several methods [34]–[36] employed Retinex theory to enhance hazy images.

A second category includes physically-based techniques. The method introduced by Fattal [8] interprets the image through a formation model that accounts for surface shading in addition to the scene transmission, and assumes that image shading and scene transmission are locally uncorrelated. The technique of Nishino *et al.* [11], [31], is a Bayesian probabilistic method that models the image with a factorial Markov random field, in which the scene albedo and depth are two statistically independent latent layers that are estimated jointly. He *et al.* [1] introduce a simple but powerful Dark Channel Prior (DCP) (the work has been extended in [37]). DCP makes it possible to roughly estimate the depth map of outdoor hazy scenes. To obtain a refined transmission map, the values of the estimate are extrapolated into the unknown regions, by a relatively computationally expensive matting strategy [38]. This prior is quite robust. As a consequence, many recent dehazing approaches [16], [22]–[24], [32], [39]–[41] have been built on the DCP. Meng *et al.* [22] introduce a patch-wise transmission estimation method derived by combining the DCP with a boundary constraint map. Tang *et al.* [16] demonstrate that, within their learning framework, the DCP is the most informative feature while other features contribute complementary information. Li *et al.* [41] employ DCP and other depth cues from stereo matching to yield superior results than conventional stereo or dehazing algorithms. A different way of local airlight estimation has been employed by Berman *et al.* [5], but only for day-time dehazing. However, as can be seen in Fig 1, the method of Berman *et al.* [5] performs poorly on night time dehazing. In recent years, neural networks have been trained to dehaze images [4], [42]–[47] by leveraging on the recent dehazing datasets [33], [48]–[50]. Their usage is, however restricted in general to day-time cases, as represented by the training set.

More recently, several techniques have been introduced to dehaze images captured in night-time conditions. Pei and Lee [17] estimate the airlight and the haze thickness by applying a color transfer function, before applying the dark channel prior [1], refined iteratively by bilateral filtering as a post-processing step. The method of Zhang *et al.* [18] estimates non-uniform incident illumination and performs color correction before using the dark channel prior. Santra and Chanda [51] have proposed to extend the color-line prior introduced in [2] to deal both with day and night-time. Zhang *et al.* [52] introduce a prior that is specific to night-time. The paper builds on a night-time hazy imaging model, which includes a local ambient illumination item. Then, it introduces a simple image prior, called the maximum reflectance prior, called the estimate the varying ambient illumination. In short, the prior assumes that, during night-time, the local maximum intensities of the color channels are mainly contributed by the ambient illumination. Li *et al.* [19] employ an optical light transmission model augmented with an atmospheric point spread function to model the glowing effect. A spatially varying atmospheric light map is also used to estimate the transmission map, based on the dark channel prior. We show in our experimental section (Fig. 8 and 9) that, whilst being among the best prior art methods, this method results in images that are too dark when the lightning is very poor.

By contrast, we introduce a dehazing technique that is able to improve visibility in both day and night-time hazy scenes. Our method is a fusion-based approach, deploying a well-studied branch of computational imaging that has found many useful applications, such as interactive photomontage [53], image editing [54], image compositing [55], HDR imaging [56], [57] and underwater imaging [58]. The main idea is to combine several images into a single one, retaining only the most significant parts of each image. In the dehazing context, multi-scale fusion was first considered only for day-time [3] and in the presence of a near-infrared (NIR) image of the same scene [59]. Compared with [3], our proposed approach, whose preliminary version was introduced in [20], derives different input images based on a local estimation of the airlight component. Moreover, as will be demonstrated in the experimental results, our technique is more robust than [3], which appears to offer limited performance in night-time conditions (please see Fig 1).

III. Local Airlight Estimation

Section III-A briefly presents the Dark Channel Prior (DCP) while section III-B introduces two original contributions.

A. Transmission Estimation

In Koschmieder's model, the transmission map $T(x)$ is directly related to the distance between the observer and the considered surface (see Eq. 3).

Following [1], and adopting the well-known dark channel prior (DCP), $T(x)$ can however be computed without resorting to depth estimation. The DCP assumes that natural objects have a weak reflectance in one of the color channels (the direct radiance is small, or dark, in at least one of the R, G, B color channels [60]), while the atmospheric intensity conveys all colors (the haze looks grey or white, i.e. all components in A_∞ are significant). Hence, assuming that A_∞ is known (we discuss estimation of it later), then $T(x)$ can be directly estimated from the weakest color (relative to atmospheric color) over a neighborhood of x. Formally, the DCP assumption states that, in most image patches, at least one color channel has some

Fig. 2. **Importance of local airlight estimation in night-time scenes**. Designed for day-time dehazing, the well-known dark channel [37] has important limitations on night scenes because it assumes a spatially constant airlight. As may be observed in the last column, our patch-based local estimate (also not refined) of the airlight is more appropriate for night-time hazy scenes. In particular, color and details that are close to light sources are better enhanced.

pixels whose intensity are close to zero. It can be written as:

$$\min_{y\in\Omega(x)}\left(\min_{c\in r,g,b}\mathcal{J}^c/{A_\infty}^c\right)=0 \tag{4}$$

with A^c_∞ denoting the component of the atmospheric light associated with color c, and $\Omega(x)$ represents a local patch centered at x. Under this assumption, the transmission can be estimated as:

$$T(x)=1-\min_{y\in\Omega(x)}\left(\min_{c\in r,g,b}\mathcal{I}^c/{A_\infty}^c\right) \tag{5}$$

B. Atmospheric Intensity Estimation

Early methods used to estimate the atmospheric intensity as the pixel color vector corresponding to the highest intensity in the image [9]. This choice was motivated by the white appearance of haze in day-time scenes. Such approach could fail, typically when a white object is selected instead of a hazy pixel. To circumvent this problem, the authors of [1] proposed to estimate the atmospheric intensity using the most haze-opaque pixels. These are defined as the ones having the brightest dark channel, i.e as the ones maximizing:

$$I_{DC}(x)=\min_{y\in\Omega(x)}\left(\min_{c\in r,g,b}\mathcal{I}^c(y)\right) \tag{6}$$

where r, g, b denote the R,G,B color channels.

This estimator works well on day-time scenes, but suffers from two weaknesses when applied to night scenes (see Fig. 2). First, it estimates the atmospheric intensity globally over the entire picture, whereas night scenes are characterized by localized and spatially non-uniform artificial illumination. Second, by maximizing the minimum over the set of color channels, it promotes those locations taking large values in all channels. It thus implicitly assumes that the atmospheric intensity is reasonably white, which is the case in day-time scenes, but is not necessarily true for night-scenes which are often characterized by strongly colored lighting.

To address those two limitations, we propose (i) to estimate the atmospheric intensity locally, within spatial neighborhoods $\Psi(x)$ around each coordinate x, and (ii) to independently compute each component of the atmospheric light. Formally, we define the local atmospheric intensity of color c, $A^c_{L\infty}(x)$, to be:

$$A^c_{L\infty}(x)=\max_{y\in\Psi(x)}\left[\min_{z\in\Omega(y)}\left(\mathcal{I}^c(z)\right)\right]=\max_{y\in\Psi(x)}\left[I^c_{MIN}(y)\right] \tag{7}$$

To motivate this formulation, we again resort to the simplified version of the Koschmieder's optical model, in which we approximate the scene radiance $\mathcal{J}^c(y)$ by the product $\rho^c(y)\cdot A^c_{L\infty}(y)$, between the normalized reflectance coefficient $\rho^c(y)$ [61] (Chapter 25) and the local illumination $A^c_{L\infty}(y)$, both values being associated to color c. Under this simplified model, we have:

$$\mathcal{I}^c(y)\approx A^c_{L\infty}(y)\cdot\rho^c(y)\cdot T(y)+A^c_{L\infty}(y)[1-T(y)] \tag{8}$$

Since both $\rho^c(y)$ and $T(y)$ lie in $[0,1]$, this equation reveals that $\mathcal{I}^c(y)$ underestimates the airlight $A^c_{L\infty}(y)$. However, when $\rho^c(y)$ tends to 1, or when $T(y)$ tends to 0, we have $\mathcal{I}^c(y)\approx A^c_{L\infty}(y)$. Interestingly, both $\rho^c(y)\to 1$ or $T(y)\to 0$ also induce an increase of $\mathcal{I}^c(y)$. Hence, assuming that $A^c_{L\infty}(y)\approx A^c_{L\infty}(x)$ due to the spatial proximity between x and y, maximizing $\mathcal{I}^c(y)$ over $\Psi(x)$ is equivalent to finding the coordinate y in the neighborhood of x for which $\mathcal{I}^c(y)$ best approximates $A^c_{L\infty}(x)$. In practice, in Equation 7, the maximization applies to $I^c_{MIN}(y)$, the minimum of $\mathcal{I}^c$ over a neighborhood of y. This is to only account for color intensities that are sufficiently representative, in the sense that these intensities (or larger ones) are observed in a sufficiently large spatial area.

The size of the neighborhood $\Psi(x)$ considered by the maximization step results from a trade-off: a large size increases the probability of including a location y where $I^c_{MIN}(y)\approx A^c_{L\infty}(y)$, but increases the risk that $A^c_{L\infty}(y)\neq A^c_{L\infty}(x)$, i.e. does not allow for fine spatial adaptation. Our experiments have revealed that a smaller Ψ patch size is generally desired in night-time conditions, as compared to day time. In practice, we recommend for night-time scenes, that the patches Ψ to be twice the size of Ω, while for day-time scenes, the size of patches Ψ be four time larger than the size of Ω. The size of Ω is typically set to 20 pixels.

Figure 3 compares the atmospheric intensity estimated by global and local strategies. Local estimation appears to capture the major changes arising from environmental illumination, while the global approach does not. More importantly, the bottom, rightmost pictures reveal the benefit of computing each atmospheric intensity component independently, as compared to searching for the location in $\Psi(x)$ maximizing the minimum over the 3 color channels, as a straightforward locally adaptive extension of [1] would do. We also observe that the image reconstructed estimated by our local method

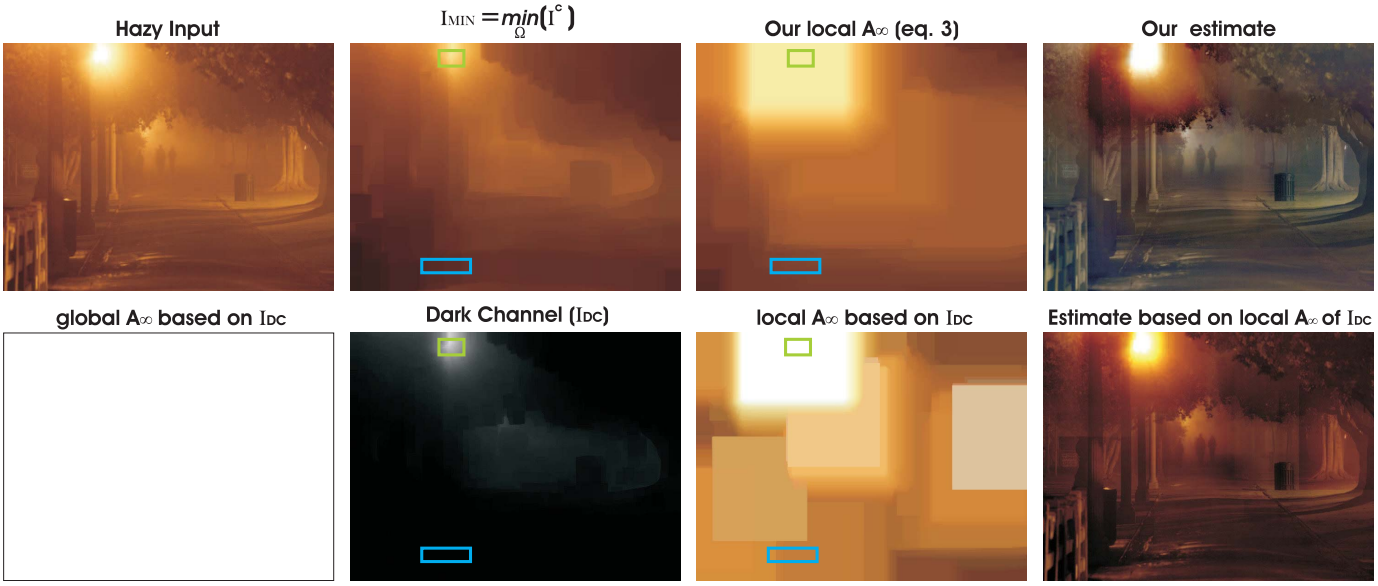

Fig. 3. **Local airlight estimation.** A global estimate of the A_∞ based on dark channel results in a white airlight (the brightest region of the dark channel is depicted here by green rectangle). As a consequence, the dark channel might become very small (see blue rectangle in second image of bottom row), which means $1 - T(x) \approx 0$ in Equation3 and no airlight influence in Equation 1. In contrast, our local airlight estimate on the same blue rectangle results in a colored atmospheric light, which in turns results in a non-unity transmission and a non-zero atmospheric light influence. Please refer to Table I that lists the concepts used in our local estimation of the A_∞.

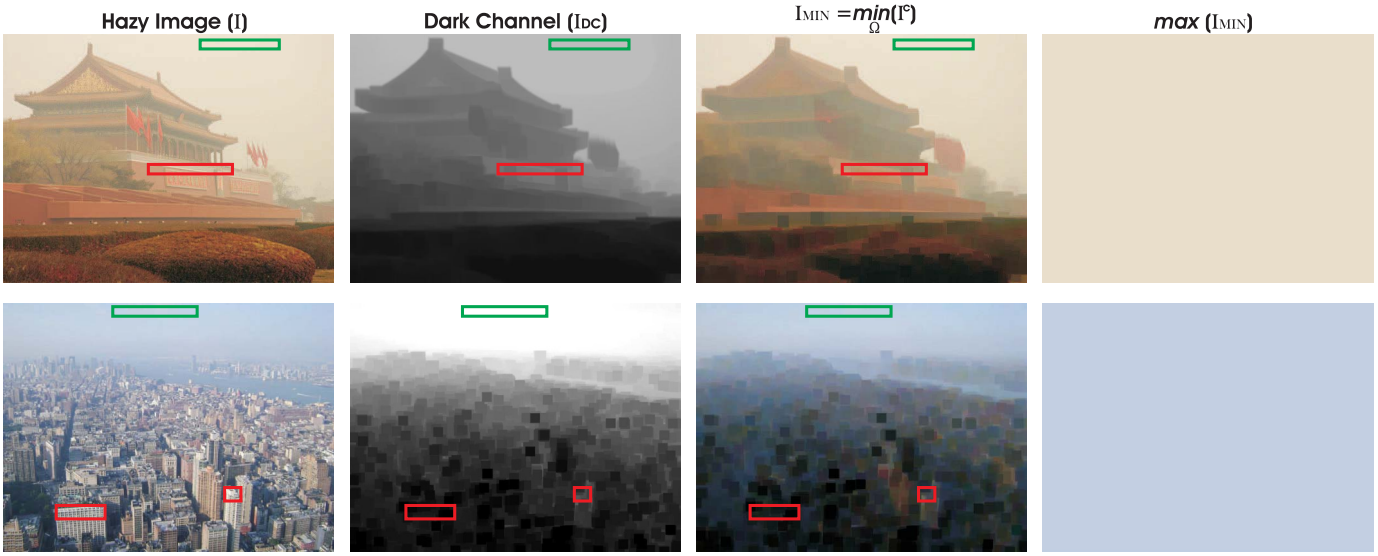

Fig. 4. **Airlight estimation**. The global version of our local airlight estimate $A^c_{L\infty}$, derived by maximizing $\min_{y\in\Omega(x)}\left(\mathcal{I}^c(y)\right)$ over the entire image, appears to be quite similar to the atmospheric intensity estimated by He *et al.* [1], from the brightest region of the dark channel (depicted by green rectangles). The red rectangles show that, in daytime scenes, the two approaches equally reject the high image intensity locations that are not relevant regarding airlight estimation. He *et al.* [1] method rejects them because the prior is dark in those regions, while our strategy rejects them because I_{MIN} gets darker than the initial image in those regions that are not subject to intense airlight illumination. Since I_{MIN} does not make any implicit assumption about the whiteness of the atmospheric illumination, it is more general than [1], especially in presence of artificial colored lighting.

of the atmospheric intensity is of better appearance (both in color and details) than those resulting from local estimation obtained based on joint processing of the color channels. Finally, it is worth noting that, when $\Psi(x)$ is defined to cover the entire image, our method reduces to a global estimator. Interestingly, in this case, Fig. 4 reveals that the global estimate of $A^c_{L\infty}$ derived by maximizing $\min_{y\in\Omega(x)}\left(\mathcal{I}^c(y)\right)$ over the entire image is quite similar to the one proposed in [1] for daytime scenes. Hence, our proposed estimator may be regarded as a night-friendly generalization of the concepts introduced in [1].

IV. Fusion Process

While the above described airlight local estimation procedure significantly improves the image enhancement process, important artifacts still arise at and around patch transitions, where color shifting and glowing defects are visible. Moreover, as detailed below, the choice of the patch size appears to

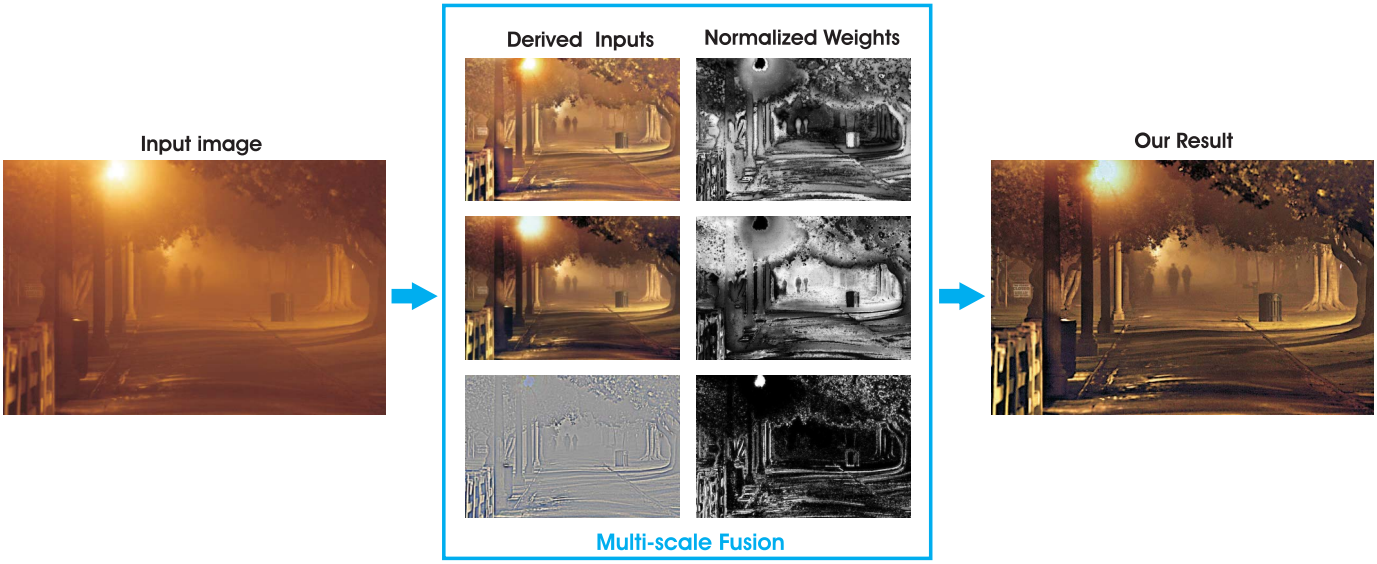

Fig. 5. **Overview of our approach.** Multi-scale fusion of the Laplacian with images dehazed from distinct airlights, estimated on spatial neighborhoods of different sizes and the corresponding normalized weight maps.

TABLE I
PARAMETERS AND CONCEPTS USED IN OUR LOCAL AIRLIGHT ESTIMATION

$\mathcal{I}(x)$	hazy image at image coordinate x (Eq. 1)
$\mathcal{J}(x)$	scene radiance or haze-free color image at coordinate x (Eq. 1)
$T(x)$	the transmission represents the fraction of light that has been transmitted from the scene surface to the observer (Eq. 1)
A_∞	atmospheric intensity (a global estimate) (Eq. 1)
A^c_∞	the c color component of the atmospheric light (Eq. 4)
$A^c_{L\infty}(x)$	the c color component of local atmospheric intensity within spatial neighborhoods $\Psi(x)$ around each coordinate x (Eq. 7)
$\Omega(x)$	represents a local patch centered at x (Eq. 4)
$I_{DC}(x)$	the Dark Channel estimate (Eq. 6)

be delicate, potentially leading to poor quality of the output images owing to non-uniformity of the airlight in night-time scenes. To circumvent this problem, we propose to adopt a multi-scale fusion approach to merge the images obtained with different patch-sizes, thereby allowing for effective and seamless enhancement of hazy night-time images.

A. Inputs

Our fusion technique is a single image approach,, meaning that it first generates multiple inputs from the original hazy image. To do this, we consider the strategy described in Section III, but use multiple patch size to locally estimate the airlight values. In short, we consider multiple patch sizes for the following reasons. The larger the patch, the more likely it will include a pixel having (close to) zero transmission, resulting in accurate airlight estimation. However, a large patch size also reduces the accuracy of spatial adjustment of the airlight, which is penalizing in the case of multiple and distinct light sources spread over the scene.

In practice, we derive two images. The **first input** is computed using a small patch size (e.g. 20×20 for an image of size 800×600), thereby preventing estimation of the airlight from multiple light sources. However the resulting input is characterized by an important loss of global contrast and chroma. We solve this limitation by computing a **second input** using larger patches (e.g. 80×80 for an image of size 800×600). This derived input considerably improves the global contrast. For completeness, we make three observations about the generation of the two inputs. First, in practice, transitions between neighboring patches are smoothed using a simple gaussian filter. Second, as a consequence of Equation7, when more than one light source is included in the region of interest, the airlight is estimated according to a winner-take-all strategy.

Third, regarding the size of the patch, we observe that it should typically increase proportionally with the resolution of the image. This is because the impact of the patch size is primarily related to the fraction of the scene covered by the patch (a patch is considered to be small if it is likely to include a single light source, while it is considered to be large when it has a high probability of including pixels having zero transmission and, consequently, with observed color equal to airlight).

As shown in Fig. 5, glowing effects are still visible in the derived inputs. To reduce such undesired effects, we derive a **third input** which is the discrete Laplacian of the original image. This input makes it possible to enhance the finest details that are transferred to the fused output.

In practice, the Laplacian is approximated by a difference of Gaussians. Specifically, we subtract from the initial image a blurred version of the image obtained using a Gaussian filter, with default standard deviation equal to two.

B. Weight Maps

Inspired by our previous fusion-based dehazing approach [3], we derive three weight maps to ensure that regions of high contrast or of high saliency will receive greater emphasis in the fusion process.

Local contrast weight is computed by applying a Laplacian filter to the luminance of each processed image. This indicator

Fig. 6. Our experiments reveal that using a small patch size (e.g. 20×20 on an image of size 800×600) gives the capability of adjusting the airlight estimation to the local light source(s). However, by compensating local illumination, such a small patch also results in an important loss of global contrast and chroma. This limitation is solved by using a larger patch (e.g. 80×80 for an image of size 800×600), which considerably improves the global contrast by maintaining a consistent airlight estimate over the entire scene. Our work proposes to improve the performance by using both of patch size alternatives, by merging the two images reconstructed from a small and a large patch size.

estimates the amount of local variation, and has been used in applications such as tone mapping [57]. It assigns high values to edges and texture variations.

Saturation weight map is computed as the standard deviation across channels at each coordinate. This factor is motivated by the fact that humans generally prefer images characterized by a high level of saturation.

Saliency weight map is computed as a difference between a Gaussian smoothed version of the input and its mean value, similarly to Achanta *et al.* [62]. This factor highlights the most conspicuous regions of an image compared with their surroundings.

C. Multi-Scale Fusion

The main goal of the fusion process is to produce an image that smoothly blends the inputs while preserving the input features highlighted by the weight maps.

The simplest way (known as *naive fusion*, or **NF**) is to directly combine the inputs and weight maps as $\mathcal{R}_{NF}(x) = \sum_k \bar{\mathcal{W}}^k(x)\mathcal{I}_k(x)$ with $\mathcal{I}_k$ being the k^{th} input and $\bar{W}^k$ denoting the normalized weight maps. The weight maps are normalized pixel-wise, i.e. on a pixel-per-pixel basis, by dividing the weight of each pixel in each map by the sum of the weights of the same pixel over all maps.

In practice, however, this naive fusion strategy has been shown to cause annoying halo artifacts, mostly at locations with strong transitions in the weight maps. Such unpleasing artifacts can be overcame by using a multi-scale Laplacian decomposition [63].

As done for other single-image dehazing approaches [3], [33], in this multiscale approach, each input $\mathcal{I}_k$ is decomposed into a Laplacian pyramid while the normalized weight maps $\bar{\mathcal{W}}^k$ are decomposed using a Gaussian pyramid. Using the same number of levels, the Gaussian and Laplacian pyramids, are independently fused at each level:

$$\mathcal{R}_l(x) = \sum_k G_l\left\{\bar{\mathcal{W}}^k(x)\right\} L_l\left\{\mathcal{I}_k(x)\right\} \tag{9}$$

where l represents the number of the pyramid levels, $L\{\mathcal{I}\}$ denotes the Laplacian of the input $\mathcal{I}$, and $G\left\{\bar{\mathcal{W}}\right\}$ is the Gaussian-smoothed normalized weight map $\bar{\mathcal{W}}$.

The fused result $\mathcal{R}$ is processed by summing the contributions from all the computed levels of the pyramid:

$$\mathcal{R}(x) = \sum_l \mathcal{R}_l(x) \uparrow^d \tag{10}$$

where $\uparrow^d$ is the upsampling operator with factor $d = 2^{l-1}$.

V. Results and Discussion

A. Day-Time Dehazing Evaluaion

In our comprehensive evaluation we first consider day-time hazy scenes. In order to perform qualitative and quantitative evaluation we test our approach on the recent O-HAZE dehazing dataset [50]. O-HAZE is a realistic datasets that consists of 45 outdoor haze-free images and their corresponding hazy version, captured in the presence of real haze, generated by professional haze machines. Fig. 7 shows several image pairs randomly selected from the O-HAZE dataset. We compare these with the specialized day-time dehazing techniques of He *et al.* [1], Meng *et al.* [22], Cai *et al.* [4], Ren *et al.* [42], Berman *et al.* [5] and $PMS-Net$ [64]. Among them Cai *et al.* [4], Ren *et al.* [42] and $PMS{-}Net$ [64] are learning-based techniques. Additionally, we compare with the night-time dehazing techniques of Li *et al.* [19], Ancuti *et al.* [20] and Zhang *et al.* [52].

On closer inspection, when comparing the dehazed images with the ground truth ones (shown in the last column), it may be observed that the DCP-based techniques of He *et al.* [1] and Meng *et al.* [22] decently restore the image structure, but introduce unpleasing color shifting, mostly in the lighter/whiter regions, where the dark channel prior generally fails. The technique of Berman *et al.* [5] is less prone to such artifacts, and leads to images with sharp edges, mostly due to its strategy to locally estimate the airlight and the transmission. Regarding the learning-based approaches, we observe that the methods of Ren *et al.* [42] and $PMS-Net$ [64] generate visually more compelling results than the deep learning approach of Cai *et al.* [4]. As expected, the specialized night-time dehazing approaches of Li *et al.* [19] and Zhang *et al.* [52] shown important limitations both in recovering the structures but also the color tones. By contrast, our technique handles color

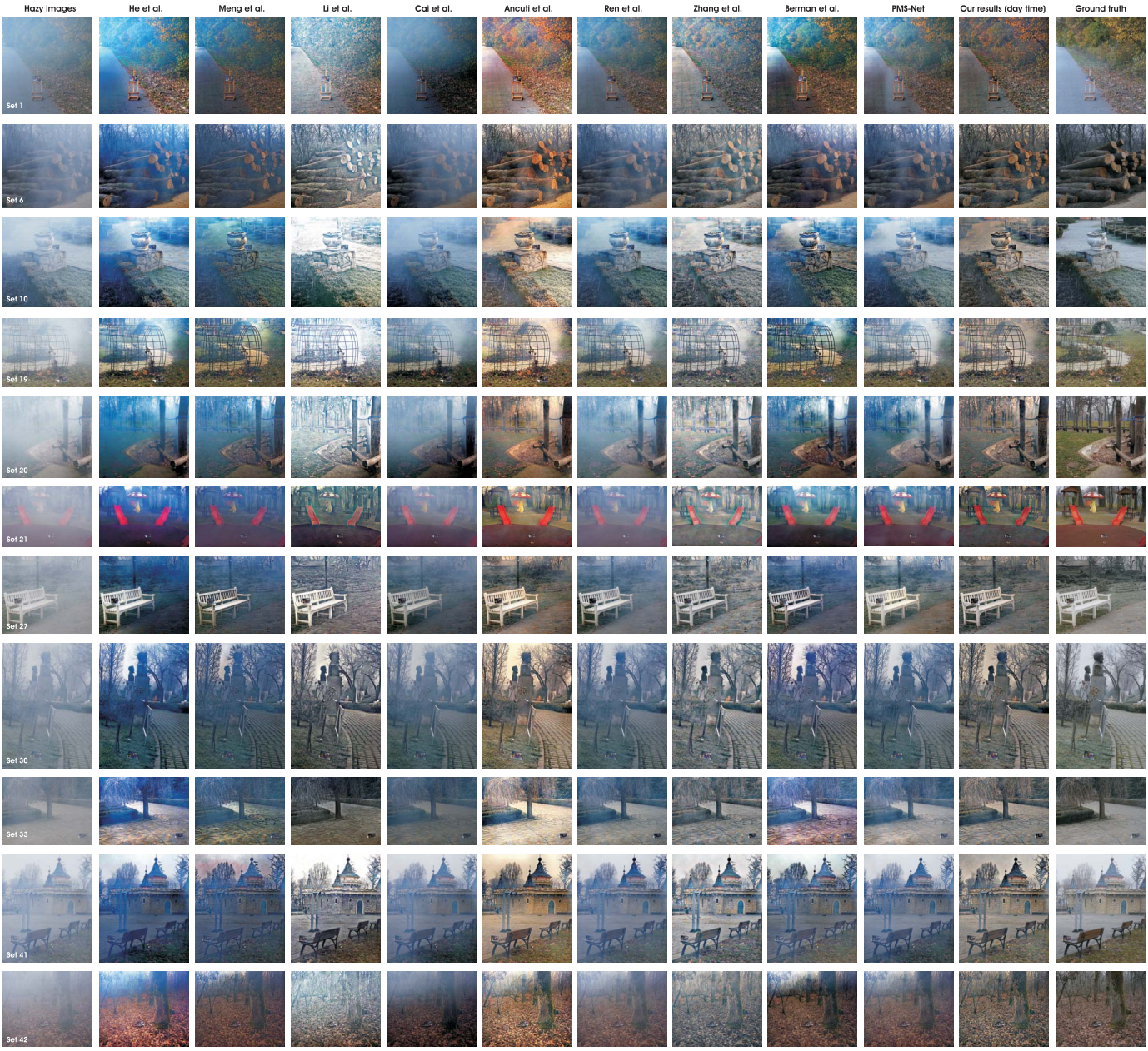

Fig. 7. **Comparative results.** The first row shows the hazy images and the last row shows the ground truth. The other rows from left to right show the results of He *et al.* [1], Meng *et al.* [22], Li *et al.* [19], Cai *et al.* [4], Ancuti *et al.* [20], Ren *et al.* [42], Zhang *et al.* [52], Berman *et al.* [5], $PMS-Net$ [64] and our results using the day-time setting.

differently than other methods, leading to higher contrast and more intense colors. It also appears to improve the initial version of our method, presented in [20] and devoted to night-time, by avoiding yellow/red color shifts.

Quantitatively, Table II and III consider three well-known metrics: PSNR, SSIM [66] and CIEDE2000 [67], [68]. Higher values indicate better quality for PSNR and SSIM, while CIEDE2000 computes the color difference between two images and generates values in the range [0,100], with smaller values indicating better color preservation. Table II presents the quantitative evaluation metrics for the image pairs shown in Fig. 7, while Table III provides the average values computed over the entire O-HAZE dataset (45 set of images).Beyond the techniques shown in Fig. 7, Table III considers as well the recent CNN-based dehazing technique $PPDN$ [43], which was the winner of the CVPR NTIRE 2018 dehazing challenge [65]. As observed qualitatively, the group of methods including He *et al.* [1], Meng *et al.* [22], Cai *et al.* [4], Berman *et al.* [5] but also the night time dehazing techniques of Li *et al.* [19] and Zhang *et al.* [52] cannot compete with our approach as well as with CNN-based techniques, both in terms of structure and color restoration. Our day-time dehazing solution, together with the learning approaches of Ren *et al.* [42], $PPDN$ [43] and $PMS-Net$ [64] appear to be the most accurate for O-HAZE quantitative evaluation. Our approach has the advantage of having a lower complexity compared with CNN-based solutions. While we can rely on the metrics and pictures provided in [43] and [64] to evaluate how CNN-based

TABLE II

QUANTITATIVE EVALUATION. WE COMPUTE THE SSIM, PSNR AND CIEDE2000 INDICES BETWEEN THE GROUND TRUTH IMAGES AND THE DEHAZED IMAGES PRODUCED BY THE EVALUATED TECHNIQUES FOR SEVERAL SETS OF IMAGES OF THE O-HAZE DATASET. THE HAZY IMAGES, GROUND TRUTH AND THE RESULTS ARE SHOWN IN FIG.7.

	He et al. [1]			**Meng et al** [22]			**Fattal** [2]			**Cai et al.** [4]			**Ancuti et al.** [20]			**Berman et al.** [5]			**Ren et al.** [43]			**Ours**		
	SSIM	**PSNR**	**CIEDE**	**SSIM**	**PSNR**	**CIEDE**	**SSIM**	**PSNR**	**CIEDE**	**SSIM**	**PSNR**	**CIEDE**	**SSIM**	**PSNR**	**CIEDE**	**SSIM**	**PSNR**	**CIEDE**	**SSIM**	**PSNR**	**CIEDE**	**SSIM**	**PSNR**	**CIEDE**
Set 1	0.82	15.64	22.37	0.77	14.51	21.06	0.73	13.24	24.29	0.58	13.01	24.42	0.75	17.27	20.09	0.76	14.09	20.97	0.81	16.79	18.17	0.82	16.62	16.87
Set 6	0.74	16.68	19.00	0.78	20.71	11.44	0.73	15.16	21.89	0.59	15.32	16.16	0.68	15.76	15.53	0.77	17.11	12.68	0.72	17.54	13.20	0.77	22.37	9.05
Set 10	0.78	16.22	15.22	0.76	15.98	16.63	0.75	16.42	17.49	0.71	15.02	16.17	0.73	14.49	19.21	0.72	14.48	17.77	0.80	16.57	13.70	0.80	19.94	11.85
Set 19	0.81	15.69	16.31	0.84	18.04	13.37	0.79	13.87	21.48	0.72	16.27	16.92	0.78	14.63	15.55	0.82	16.80	14.49	0.83	17.36	12.94	0.85	19.79	10.52
Set 20	0.61	16.49	23.81	0.72	17.86	20.91	0.62	15.62	20.73	0.50	13.69	23.71	0.78	18.01	12.67	0.72	15.89	19.40	0.63	15.05	20.98	0.80	20.07	11.69
Set 21	0.69	16.78	27.50	0.78	19.80	21.13	0.63	16.10	28.25	0.71	16.37	19.49	0.78	19.49	10.72	0.72	15.90	20.54	0.73	17.14	20.26	0.77	22.70	12.51
Set 27	0.61	13.60	21.38	0.68	15.24	18.76	0.67	14.18	22.37	0.64	15.21	17.16	0.77	19.02	10.94	0.70	16.09	18.41	0.71	18.11	14.16	0.76	19.24	10.26
Set 30	0.75	15.71	18.85	0.74	14.68	18.59	0.72	14.68	18.46	0.77	18.57	12.70	0.83	21.51	11.25	0.81	17.48	14.55	0.82	19.72	12.66	0.84	19.89	10.65
Set 33	0.76	18.96	18.54	0.74	18.01	15.84	0.76	17.28	17.86	0.81	17.87	14.61	0.61	12.15	20.86	0.66	16.37	19.39	0.88	22.61	10.87	0.76	20.06	9.75
Set 41	0.77	15.42	19.54	0.72	13.37	21.45	0.66	12.52	23.71	0.84	20.03	12.78	0.84	18.97	13.02	0.82	16.49	14.36	0.88	20.91	12.34	0.85	17.43	11.24
Set 42	0.79	15.47	19.70	0.82	20.08	11.03	0.73	17.83	13.21	0.58	16.35	15.58	0.74	14.60	15.37	0.82	17.56	11.00	0.72	16.74	12.87	0.85	23.04	8.53

TABLE III

QUANTITATIVE EVALUATION OF ALL THE 45 SET OF IMAGES OF THE O-HAZE DATASET. THIS TABLE PRESENTS THE AVERAGE VALUES OF THE SSIM, PSNR AND CIEDE2000 INDEXES, OVER THE ENTIRE DATASET. BEYOND THE TECHNIQUES SHOWN IN FIG. 7, WE ALSO COMPARED AGAINST THE WINNER OF THE CVPR NTIRE 2018 DEHAZING CHALLENGE [65], [69]

	He et al. [1]	**Meng et al.** [22]	**Li et al.** [19]	**Cai et al.** [4]	**Ancuti et al.** [20]	**Ren et al.** [43]	**Zhang et al.** [53]	**Berman et al.** [5]	**PPDN** [67]	**PMS-Net** [65]	**Ours**
SSIM	0.735	0.753	0.678	0.666	0.747	0.765	0.704	0.75	0.777	**0.814**	0.795
PSNR	16.586	17.443	15.034	16.207	16.855	19.068	17.091	16.61	**24.598**	19.045	20.159
CIEDE2000	20.745	16.968	18.211	17.348	16.431	14.67	14.816	17.088	12.124	13.467	**11.56**

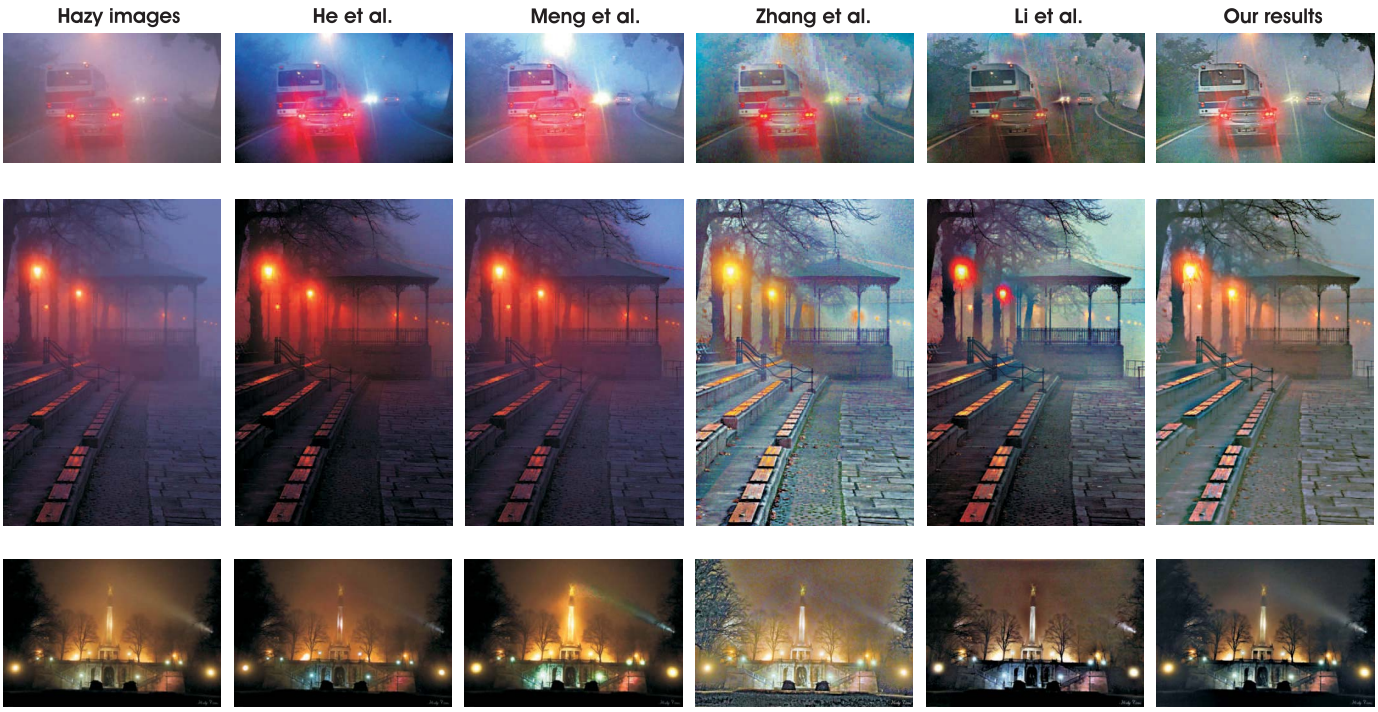

Fig. 8. **Comparative results for night-time hazy scenes.** We compare with the day-time dehazing techniques of He *et al.* [1], Meng *et al.* [22] but also with the specialized night-time dehazing methods of Zhang *et al.* [18] and Li *et al.* [19].

methods deal with the O-Haze dataset, the code for those CNN-based methods is not available and could not be tested on night-time images. However, we might reasonably expect that models trained on day-time images do not generalize well to night-time scenes (see for example the issues raised when transferring models between domains [70]). By contrast, our method has the advantage of also being competitive also for night-time dehazing, as shown in the following.

B. Night-Time Dehazing Evaluation

We also tested our approach on the dataset introduced in [19] that contains various quality and formats of images taken of night-time scenes. We compared our method with the recent night-time dehazing techniques of Zhang *et al.* [18], Li *et al.* [19] and Zhang *et al.* [52] and also with the day-time dehazing methods of Ancuti and Ancuti [3], Fattal [2], He *et al.* [1], Meng *et al.* [22] and Berman *et al.* [5] . For all results we used the original code provided by the authors on their webpages.

Figures 1, 8 and 9 demonstrate the limitations of the day-time dehazing techniques of Ancuti [3], Fattal [2], He *et al.* [1], Meng *et al.* [22] and Berman *et al.* [5] when applied to night-time hazy images. In general these techniques are not able to restore color well, and only slightly remove the haze for such scenes. Figures 8 and 9 directly compare our approach with the recent specialized techniques of Li *et al.* [19] and

Fig. 9. **Comparative results for night-time hazy scenes.** We compare with the day-time dehazing techniques of Meng *et al.* [22] and Berman *et al.* [5] but also with the specialized night-time dehazing methods of Li *et al.* [19] and Zhang *et al.* [52] .

TABLE IV

EVALUATION OF THE RESULTS IN FIG. 10 BASED ON THE PSNR VALUES COMPUTED AS AN AVERAGE ON RGB COMPONENTS FOR EACH OF THE 6 COLORS OF THE REFERENCE PALETTE

	yellow	white	brown	red	blue	green	**average**
Fattal [2]	21.10	23.94	15.43	20.71	15.12	15.77	18.68
Ancuti [3]	17.75	15.82	13.49	19.16	14.01	17.01	16.20
Zhang et al. [18]	21.20	23.21	**21.30**	20.10	15.38	12.66	18.98
Li et al. [19]	19.80	23.21	16.94	**23.38**	**17.69**	**21.09**	20.35
Our method	**27.33**	**30.04**	18.58	23.21	17.59	17.66	**22.40**

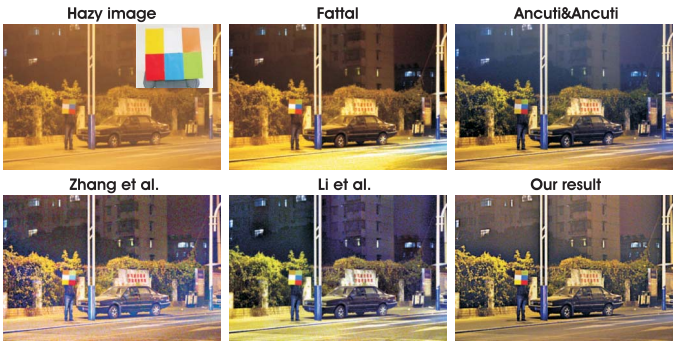

Fig. 10. **Comparative results on the image with color checker provided by Zhang *et al.* [18].** The night-time hazy image with color palette (top-left) is enhanced by several dehazing techniques. See Table IV for the PSNR values.

Zhang *et al.* [18]. The method of Li *et al.* [19] tends to darken the original image and to over-amplify colors in some regions. Whilst much better than day-time methods, the strategy of Zhang *et al.* [52] sometimes appears to generate less contrasted images than our approach (see in particular the dark scenes presented in the second and fourth lines of Fig. 9).

Moreover, our approach has the advantage of simplicity and computational efficiency. Our unoptimized Matlab implementation processes an 800×600 image in less than 4 seconds. The method of Li *et al.* [19] computes results on a similar image in more than 30 seconds, while the method of Zhang *et al.* [18] requires a similar computation as He *et al.* [1] (approx. 20 seconds per image).

We also performed a quantitative evaluation using the pair of images provided by Zhang *et al.* [18]. The left side of the top row of Fig. 10 shows the reference color palette and the night-time hazy image containing this palette. We processed this input image using several different dehazing techniques [2], [3], [18], [19] and computed the PSNR values for each of the 6 colors (shown in Table IV). As can be seen, our approach generally performs better in terms of PSNR as compared with the other techniques.

VI. CONCLUSIONS

In this paper we introduce an effective technique to enhance both day-time and night-time hazy scenes. Our method removes the haze by inverting the simplified Koschmieder's light transmission model. Therefore it has to estimate the airlight. In contrast to most previous works, we estimate the airlight on local patches (and not on the whole image), since under night-time conditions, the lighting generally arises from multiple artificial sources, and is thus intrinsically non-uniform. To circumvent the patch-size selection issue, we propose to fusion multiple instances of inverted images, obtained with distinct patch sizes. An additional input, computed by a Laplace operator, is provided to the fusion process to reduce the glowing effects and emphasize the finest image details. During fusion, the derived inputs are blended in a

multi-scale fashion using a Laplacian pyramid decomposition. The experimental results demonstrate the superiority of our approach compared with the recent techniques both for day and night time hazy scenes.

REFERENCES

[1] K. He, J. Sun, and X. Tang, "Single image haze removal using dark channel prior," in *Proc. IEEE CVPR*, Jun. 2009, pp. 1956–1963.

[2] R. Fattal, "Dehazing using color-lines," *ACM Trans. Graph.*, vol. 34, no. 1, pp. 1–14, Dec. 2014.

[3] C. O. Ancuti and C. Ancuti, "Single image dehazing by multi-scale fusion," *IEEE Trans. Image Process.*, vol. 22, no. 8, pp. 3271–3282, Aug. 2013.

[4] B. Cai, X. Xu, K. Jia, C. Qing, and D. Tao, "DehazeNet: An end-to-end system for single image haze removal," *IEEE Trans. Image Process.*, vol. 25, no. 11, pp. 5187–5198, Nov. 2016.

[5] D. Berman, T. Treibitz, and S. Avidan, "Single image dehazing using haze-lines," *IEEE Trans. Pattern Anal. Mach. Intell.*, vol. 42, no. 3, pp. 720–734, Mar. 2020.

[6] J. Kopf *et al.*, "Deep photo: Model-based photograph enhancement and viewing," in *Proc. ACM SIGGRAPH Asia Papers (SIGGRAPH Asia)*, 2008, Art. no. 116.

[7] S. G. Narasimhan and S. K. Nayar, "Contrast restoration of weather degraded images," *IEEE Trans. Pattern Anal. Mach. Intell.*, vol. 25, no. 6, pp. 713–724, Jun. 2003.

[8] R. Fattal, "Single image dehazing," in *Proc. ACM SIGGRAPH Papers (SIGGRAPH)*, 2008, Art. no. 72.

[9] R. T. Tan, "Visibility in bad weather from a single image," in *Proc. IEEE Conf. Comput. Vis. Pattern Recognit.*, Jun. 2008, pp. 1–8.

[10] J.-P. Tarel and N. Hautiere, "Fast visibility restoration from a single color or gray level image," in *Proc. IEEE 12th Int. Conf. Comput. Vis.*, Sep. 2009, pp. 2201–2208.

[11] L. Kratz and K. Nishino, "Factorizing scene albedo and depth from a single foggy image," in *Proc. IEEE ICCV*, Sep. 2009, pp. 1701–1708.

[12] C. Orniana Ancuti, C. Ancuti, and P. Bekaert, "Effective single image dehazing by fusion," in *Proc. IEEE Int. Conf. Image Process.*, Sep. 2010, pp. 3541–3544.

[13] C. O. Ancuti, C. Ancuti, C. Hermans, and P. Bekaert, "A fast semi-inverse approach to detect and remove the haze from a single image," in *Proc. ACCV*, 2010, pp. 501–514.

[14] C. Ancuti and C. O. Ancuti, "Effective contrast-based dehazing for robust image matching," *IEEE Geosci. Remote Sens. Lett.*, vol. 11, no. 11, pp. 1871–1875, Nov. 2014.

[15] S. Emberton, L. Chittka, and A. Cavallaro, "Hierarchical rank-based veiling light estimation for underwater dehazing," in *Proc. Brit. Mach. Vis. Conf.*, 2015, pp. 1–12.

[16] K. Tang, J. Yang, and J. Wang, "Investigating haze-relevant features in a learning framework for image dehazing," in *Proc. IEEE Conf. Comput. Vis. Pattern Recognit.*, Jun. 2014, pp. 2995–3002.

[17] S.-C. Pei and T.-Y. Lee, "Nighttime haze removal using color transfer pre-processing and dark channel prior," in *Proc. 19th IEEE Int. Conf. Image Process.*, Sep. 2012, pp. 957–960.

[18] J. Zhang, Y. Cao, and Z. Wang, "Nighttime haze removal based on a new imaging model," in *Proc. IEEE Int. Conf. Image Process. (ICIP)*, Oct. 2014, pp. 4557–4561.

[19] Y. Li, R. T. Tan, and M. S. Brown, "Nighttime haze removal with glow and multiple light colors," in *Proc. IEEE Int. Conf. Comput. Vis. (ICCV)*, Dec. 2015, pp. 226–234.

[20] C. Ancuti, C. O. Ancuti, C. De Vleeschouwer, and A. C. Bovik, "Night-time dehazing by fusion," in *Proc. IEEE Int. Conf. Image Process. (ICIP)*, Sep. 2016, pp. 2256–2260.

[21] H. Koschmieder, "Theorie der horizontalen sichtweite," *Beitrage zur Physik der Freien Atmosphare*, vol. 12, pp. 171–181, Oct. 1924.

[22] G. Meng, Y. Wang, J. Duan, S. Xiang, and C. Pan, "Efficient image dehazing with boundary constraint and contextual regularization," in *Proc. IEEE Int. Conf. Comput. Vis.*, Dec. 2013, pp. 617–624.

[23] Y.-H. Lai, Y.-L. Chen, C.-J. Chiou, and C.-T. Hsu, "Single-image dehazing via optimal transmission map under scene priors," *IEEE Trans. Circuits Syst. Video Technol.*, vol. 25, no. 1, pp. 1–14, Jan. 2015.

[24] Z. Li and J. Zheng, "Edge-preserving decomposition-based single image haze removal," *IEEE Trans. Image Process.*, vol. 24, no. 12, pp. 5432–5441, Dec. 2015.

[25] S. K. Nayar and S. G. Narasimhan, "Vision in bad weather," in *Proc. 7th IEEE Int. Conf. Comput. Vis.*, Sep. 1999, pp. 820–827.

[26] S. G. Narasimhan and S. K. Nayar, "Chromatic framework for vision in bad weather," in *Proc. IEEE Conf. Comput. Vis. Pattern Recognit. (CVPR)*, Jun. 2000, pp. 598–605.

[27] S. Shwartz, E. Namer, and Y. Y. Schechner, "Blind haze separation," in *Proc. IEEE Comput. Soc. Conf. Comput. Vis. Pattern Recognit. (CVPR)*, Jun. 2006, pp. 1984–1991.

[28] T. Treibitz and Y. Y. Schechner, "Polarization: Beneficial for visibility enhancement?" in *Proc. IEEE Conf. Comput. Vis. Pattern Recognit.*, Jun. 2009, pp. 525–532.

[29] Y. Y. Schechner and Y. Averbuch, "Regularized image recovery in scattering media," *IEEE Trans. Pattern Anal. Mach. Intell.*, vol. 29, no. 9, pp. 1655–1660, Sep. 2007.

[30] E. Namer, S. Shwartz, and Y. Y. Schechner, "Skyless polarimetric calibration and visibility enhancement," *Opt. Express*, vol. 17, no. 2, pp. 472–493, Jan. 2009.

[31] K. Nishino, L. Kratz, and S. Lombardi, "Bayesian defogging," *Int. J. Comput. Vis.*, vol. 98, no. 3, pp. 263–278, Jul. 2012.

[32] Y. Gao, H.-M. Hu, S. Wang, and B. Li, "A fast image dehazing algorithm based on negative correction," *Signal Process.*, vol. 103, pp. 380–398, Oct. 2014.

[33] L. Kwon Choi, J. You, and A. C. Bovik, "Referenceless prediction of perceptual fog density and perceptual image defogging," *IEEE Trans. Image Process.*, vol. 24, no. 11, pp. 3888–3901, Nov. 2015.

[34] A. Galdran, J. Vazquez-Corral, D. Pardo, and M. Bertalmío, "Enhanced variational image dehazing," *SIAM J. Imag. Sci.*, vol. 8, no. 3, pp. 1519–1546, Jan. 2015.

[35] Y. Wang, H. Wang, C. Yin, and M. Dai, "Biologically inspired image enhancement based on retinex," *Neurocomputing*, vol. 177, pp. 373–384, Feb. 2016.

[36] A. Galdran, A. Bria, A. Alvarez-Gila, J. Vazquez-Corral, and M. Bertalmio, "On the duality between retinex and image dehazing," in *Proc. IEEE/CVF Conf. Comput. Vis. Pattern Recognit.*, Jun. 2018, pp. 8212–8221.

[37] K. He, J. Sun, and X. Tang, "Single image haze removal using dark channel prior," *IEEE Trans. Pattern Anal. Mach. Intell.*, vol. 33, no. 12, pp. 2341–2353, Dec. 2011.

[38] A. Levin, D. Lischinski, and Y. Weiss, "A closed form solution to natural image matting," in *Proc. IEEE Comput. Soc. Conf. Comput. Vis. Pattern Recognit. (CVPR)*, Jun. 2006, pp. 61–68.

[39] Q. Zhu, J. Mai, and L. Shao, "A fast single image haze removal algorithm using color attenuation prior," *IEEE Trans. Image Process.*, vol. 24, no. 11, pp. 3522–3533, Nov. 2015.

[40] J.-B. Wang, N. He, L.-L. Zhang, and K. Lu, "Single image dehazing with a physical model and dark channel prior," *Neurocomputing*, vol. 149, pp. 718–728, Feb. 2015.

[41] Z. Li, P. Tan, R. T. Tan, D. Zou, S. Z. Zhou, and L.-F. Cheong, "Simultaneous video defogging and stereo reconstruction," in *Proc. IEEE Conf. Comput. Vis. Pattern Recognit. (CVPR)*, Jun. 2015, pp. 4988–4997.

[42] W. Ren, S. Liu, H. Zhang, J. Pan, X. Cao, and M.-H. Yang, "Single image dehazing via multi-scale convolutional neural networks," in *Proc. Eur. Conf. Comput. Vis.*, 2016, pp. 154–169.

[43] H. Zhang, V. Sindagi, and V. M. Patel, "Multi-scale single image dehazing using perceptual pyramid deep network," in *Proc. IEEE/CVF Conf. Comput. Vis. Pattern Recognit. Workshops (CVPRW)*, Jun. 2018, pp. 902–911.

[44] W. Ren *et al.*, "Gated fusion network for single image dehazing," in *Proc. IEEE/CVF Conf. Comput. Vis. Pattern Recognit.*, Jun. 2018, pp. 3253–3261.

[45] W. Ren, J. Pan, H. Zhang, X. Cao, and M.-H. Yang, "Single image dehazing via multi-scale convolutional neural networks with holistic edges," *Int. J. Comput. Vis.*, vol. 128, no. 1, pp. 240–259, Jan. 2020.

[46] R. Liu, L. Ma, Y. Wang, and L. Zhang, "Learning converged propagations with deep prior ensemble for image enhancement," *IEEE Trans. Image Process.*, vol. 28, no. 3, pp. 1528–1543, Mar. 2019.

[47] A. Wang, W. Wang, J. Liu, and N. Gu, "AIPNet: Image-to-image single image dehazing with atmospheric illumination prior," *IEEE Trans. Image Process.*, vol. 28, no. 1, pp. 381–393, Jan. 2019.

[48] C. Ancuti, C. O. Ancuti, and C. De Vleeschouwer, "D-HAZY: A dataset to evaluate quantitatively dehazing algorithms," in *Proc. IEEE Int. Conf. Image Process. (ICIP)*, Sep. 2016, pp. 2226–2230.

[49] B. Li *et al.*, "Benchmarking single-image dehazing and beyond," *IEEE Trans. Image Process.*, vol. 28, no. 1, pp. 492–505, Jan. 2019.

[50] C. O. Ancuti, C. Ancuti, R. Timofte, and C. De Vleeschouwer, "O-HAZE: A dehazing benchmark with real hazy and haze-free outdoor images," in *Proc. IEEE/CVF Conf. Comput. Vis. Pattern Recognit. Workshops (CVPRW)*, Jun. 2018, pp. 754–762.

[51] S. Santra and B. Chanda, "Day/night unconstrained image dehazing," in *Proc. 23rd Int. Conf. Pattern Recognit. (ICPR)*, Dec. 2016, pp. 1406–1411.

[52] J. Zhang, Y. Cao, S. Fang, Y. Kang, and C. W. Chen, "Fast haze removal for nighttime image using maximum reflectance prior," in *Proc. IEEE Conf. Comput. Vis. Pattern Recognit. (CVPR)*, Jul. 2017, pp. 7418–7426.

[53] A. Agarwala *et al.*, "Interactive digital photomontage," *ACM Trans. Graph.*, vol. 23, no. 3, p. 294, Aug. 2004.

[54] P. Pérez, M. Gangnet, and A. Blake, "Poisson image editing," *ACM Trans. Graph.*, vol. 22, no. 3, p. 313, Jul. 2003.

[55] M. Grundland, R. Vohra, G. P. Williams, and N. A. Dodgson, "Cross dissolve without cross fade," *Comput. Graph. Forum*, vol. 6, no. 25, p. 3, 2006.

[56] P. J. Burt and R. J. Kolczynski, "Enhanced image capture through fusion," in *Proc. 4th Int. Conf. Comput. Vis.*, May 1993, pp. 173–182.

[57] T. Mertens, J. Kautz, and F. V. Reeth, "Exposure fusion," *Comp. Graph. Forum*, 2009.

[58] C. Ancuti, C. O. Ancuti, T. Haber, and P. Bekaert, "Enhancing underwater images and videos by fusion," in *Proc. IEEE Conf. Comput. Vis. Pattern Recognit.*, Jun. 2012, pp. 81–88.

[59] L. Schaul, C. Fredembach, and S. Susstrunk, "Color image dehazing using the near-infrared," in *Proc. 16th IEEE Int. Conf. Image Process. (ICIP)*, Nov. 2009, pp. 1629–1632.

[60] P. S. Chavez, "An improved dark-object subtraction technique for atmospheric scattering correction of multispectral data," *Remote Sens. Environ.*, vol. 24, no. 3, pp. 459–479, Apr. 1988.

[61] M. Bass, *Handbook of Optics: Devices, Measurements, and Properties*, vol. 2, 2nd ed. New York, NY, USA: McGraw-Hill, 1995.

[62] R. Achanta, S. Hemami, F. Estrada, and S. Susstrunk, "Frequency-tuned salient region detection," in *Proc. IEEE Conf. Comput. Vis. Pattern Recognit.*, Jun. 2009, pp. 1597–1604.

[63] P. Burt and T. Adelson, "The Laplacian pyramid as a compact image code," *IEEE Trans. Commun.*, vol. COM-31, no. 4, pp. 532–540, Apr. 1983.

[64] W.-T. Chen, J.-J. Ding, and S.-Y. Kuo, "PMS-net: Robust haze removal based on patch map for single images," in *Proc. IEEE/CVF Conf. Comput. Vis. Pattern Recognit. (CVPR)*, Jun. 2019, pp. 11681–11689.

[65] C. Ancuti *et al.*, "NTIRE 2018 challenge on image dehazing: Methods and results," in *Proc. IEEE/CVF Conf. Comput. Vis. Pattern Recognit. Workshops (CVPRW)*, Jun. 2018, pp. 1004–100410.

[66] Z. Wang, A. C. Bovik, H. R. Sheikh, and E. P. Simoncelli, "Image quality assessment: From error visibility to structural similarity," *IEEE Trans. Image Process.*, vol. 13, no. 4, pp. 600–612, Apr. 2004.

[67] G. Sharma, W. Wu, and E. N. Dalal, "The CIEDE2000 color-difference formula: Implementation notes, supplementary test data, and mathematical observations," *Color Res. Appl.*, vol. 30, no. 1, pp. 21–30, Feb. 2005.

[68] S. Westland, C. Ripamonti, and V. Cheung, *Computational Colour Science Using MATLAB*, 2nd ed. Hoboken, NJ, USA: Wiley, 2012.

[69] C. Ancuti *et al.*, "Ntire 2019 challenge on image dehazing: Methods and results," in *Proc. IEEE CVPR, NTIRE Workshop*, Jun. 2018, pp. 891–901.

[70] J. Hoffman *et al.*, "Cycada: Cycle-consistent adversarial domain adaptation," in *Proc. Int. Conf. Mach. Learn.*, 2018, pp. 1–15.